
CHALMERS
UNIVERSITY OF TECHNOLOGY

# Power-Response Matrix-Based Modeling of Converter Systems for Small-Signal Analysis

# Power-Response Matrix-Based Modeling of Converter Systems for Small-Signal Analysis


Anant Narula
*Dept. of Electrical Engineering*
*Chalmers University of Technology*
Göteborg, Sweden
anant.narula@chalmers.se

Paul Imgart
*Dept. of Electrical Engineering*
*Chalmers University of Technology*
Göteborg, Sweden
paul.imgart@chalmers.se

Massimo Bongiorno
*Dept. of Electrical Engineering*
*Chalmers University of Technology*
Göteborg, Sweden
massimo.bongiorno@chalmers.se

Paolo Mattavelli
*Dept. of Management and Engineering*
*University of Padova*
Vicenza, Italy
paolo.mattavelli@unipd.it

Mebtu Beza
*Dept. of Electrical Engineering*
*Chalmers University of Technology*
Göteborg, Sweden
mebtu.beza@chalmers.se

Jan R. Svensson
*Hitachi Energy Research*
*Hitachi Energy*
Västerås, Sweden
jan.r.svensson@hitachienergy.com



***Abstract*—In this paper, a novel small-signal modeling approach for grid-connected converter systems is presented. The approach is based on the converter system's power-response matrix, which correlates variations in grid voltage magnitude and frequency with variations in the exchanged active and reactive powers from the converter system. This formulation is useful not only for small-signal stability analysis of interconnected systems but also for directly assessing the grid services offered by converter systems, such as their contributions to total system inertia and damping. The paper provides a detailed analytical derivation of the converter system's power-response matrix, along with an analysis of the small-signal stability of the interconnected system. Furthermore, a comparison between the proposed power-response matrix-based model and the more conventional impedance-based model is presented, establishing the equivalence between the two modeling approaches and highlighting the advantages of the proposed approach.**



***Index Terms*—Frequency variation, grid-forming converter, impedance model, small-signal stability, voltage variation.**


## I. Introduction

The prevalent method to study the stability of a power system with grid-connected converters is to separate the system into two subsystems, one containing the grid ("source" subsystem) and other the converter ("load" subsystem) [1]. As these two subsystems are solely coupled through the bus voltage at the point-of-common-coupling (PCC) and the exchanged current, the knowledge of the small-signal terminal characteristics of both subsystems is sufficient to study the small-signal stability of the interconnected system. The small-signal terminal characteristics are typically expressed as the source output impedance and the converter input admittance; the generalized Nyquist criterion (GNC) can thus be applied to their product to determine the small-signal stability of the interconnected system [2], [3]. For this, the subsystems need to be modeled in a common reference frame.

As it relates to the physical behaviour of the system, the results of the stability study have to be independent of the selected reference frame. Therefore, the subsystems are typically modelled in a synchronous reference frame (SRF) for convenience [1]. The proliferation of converter-interfaced generation units results in a frequency weak system due to decreasing system inertia, while grid-forming (GFM) converters introduce additional frequency dynamics into the power system. As a consequence, changes in the frequency of the PCC voltage should not be neglected. A number of studies describe the inclusion of frequency dynamics in the small-signal models [4]–[8]. The proposed solution in these studies involves small-signal modeling in a SRF, which is defined by either the rated angular frequency [6] or the fundamental angular frequency of the PCC voltage [4], [5], [7], [8].

This paper introduces an equivalent and alternative approach to impedance-based modeling of grid-connected converter systems for small-signal studies. The proposed approach models a converter system using its *power-response matrix*, which relates variations in the active and reactive power of the converter system to variations in grid voltage magnitude and frequency. This formulation enables the direct assessment of grid services (also referred to as GFM properties) offered by the converter system, such as synthetic inertia and damping. Hence, the proposed formulation closely aligns with methods such as the network frequency perturbation response [9], [10] used by system operators to evaluate the frequency stability and GFM properties of converter systems. Moreover, it is also useful for analyzing the reactive power response of the converter system to grid voltage variations and the coupling between active and reactive power responses. Finally, the power-response matrix, being independent of the selected reference frame, offers simplicity over the conventional impedance-based modeling approach when aggregating subsystems to analyze the small-signal stability of large interconnected systems.

## II. System and Controller Descriptions

Figure 1 shows the single-line diagram of the grid-connected converter system together with the block scheme of the

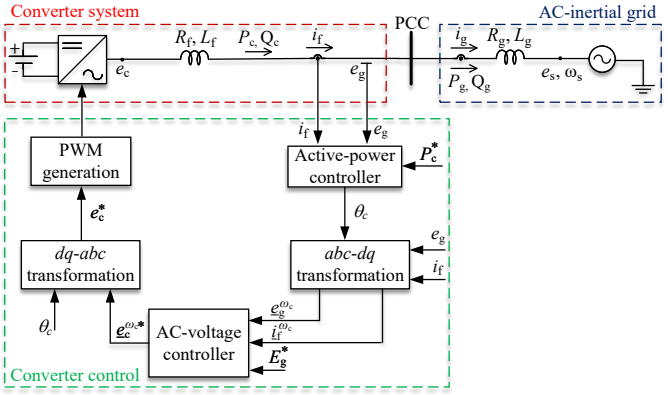


Fig. 1. Single-line diagram of considered grid-connected converter system and block scheme of implemented GFM control.

implemented controller. The grid model consists of an ideal voltage source behind a grid impedance, with resistance $R_g$ and inductance $L_g$. The three-phase voltage at the voltage source is denoted by $e_s$, while the voltage at the PCC and the converter's terminal are denoted by $e_g$ and $e_c$, respectively. The quantities $P_c$ and $Q_c$ represent the active and reactive power output of the converter system; whereas, $P_g$ and $Q_g$ represent the active and reactive power injected to the grid, respectively. The variables $i_f$ and $i_g$ denote the three-phase current across the converter filter and the grid, respectively. For the considered system, $P_c = P_g$, $Q_c = Q_g$, and $i_f = i_g$. The magnitude of the source voltage is assumed constant; whereas, to account for inertia and to model frequency dynamics in the grid, the angular frequency of the voltage source, $\omega_s$, is obtained using the swing equation as follows

$$\omega_s = \overbrace{\left(\frac{1}{\frac{2H}{\omega_N}s + \frac{K_D}{\omega_N}}\right)}^{G'_{pc}} \frac{(P_g - P_g^\star)}{S_N} + \omega_N. \tag{1}$$

The terms $\omega_N$ and $S_N$ denote the rated/nominal angular frequency of the system and the rated power of the converter, respectively. $H$ and $K_D$ represent the inertia time-constant (in seconds) and mechanical damping coefficient (in per unit) of the grid, respectively. The term $s$ is the Laplace-transform variable, interpreted as $d/dt$ where appropriate, and "$\star$" denotes a reference signal in the notations.

A grid-forming (GFM) control is adopted for the converter system, based on the direct control of converter voltage (DCCV) approach from [11]. In this control strategy, an AC voltage controller[1] (AVC) regulates the magnitude of the voltage at the PCC and calculates the reference value of the converter voltage magnitude, $E_c^\star$, while an active power controller (APC) calculates the converter voltage angle, $\theta_c$. All controllers are designed in the converter *dq*-frame (using power-invariant transformation), defined by the angle output of the APC.

[1]Alternatively, a reactive power controller can be used, depending on the system's requirements

The AVC implemented here comprises a pure integrator. Accordingly, the reference value for the converter voltage vector, $\underline{e}_c^{\omega_c\star}$, is calculated as follows [11]

$$\underline{e}_c^{\omega_c\star} = E_N + \overbrace{\frac{K_{i,vc}}{s}}^{G_{vc}}\left(E_g^\star - \overbrace{\frac{\alpha_{lpf}}{s+\alpha_{lpf}}}^{G_{lpf}} E_g\right) - \overbrace{\frac{s}{s+\alpha_{hpf}}}^{G_{hpf}} R'_a \underline{i}_f^{\omega_c}, \tag{2}$$

where $E_N$ denotes the rated line-to-line voltage of the system and $E_g$ denotes magnitude of the measured line-to-line voltage at the PCC. The superscript "$\omega_c$" is used to represent entities in the converter *dq*-frame. The term $\alpha_{lpf}$ denotes the cut-off frequency of the low-pass filter for the PCC voltage measurement. A transient damping term comprising a high-pass filtered converter current is added at the output of the AVC to prevent a poorly damped closed-loop system. $R'_a$ denotes the active resistance, and $\alpha_{hpf}$ the cutoff frequency of the high-pass filter, with values selected as suggested in [11]. The integral gain of the controller, $K_{i,vc}$, can be calculated using the loop-shaping approach as, $K_{i,vc} = \frac{\alpha_{vc}(X_f+\hat{X}_g)}{(\hat{X}_g)}$, where $\alpha_{vc}$ denotes the desired closed-loop bandwidth (in rad/s) of the first-order response from $E_g^\star$ to $E_g$. $X$ denotes the reactance of the corresponding inductance. To guarantee the desired response speed for all grid conditions, $\hat{X}_g$ is typically set for the strongest grid strength provided by the system operator [11].

For the investigated GFM control, the APC provides both active power reference tracking and grid synchronization. The implemented APC consists of a proportional-integral regulator for accurate reference tracking and an active damping term, $R_a$, to improve the controller's dynamic performance. The APC calculates the converter voltage angle as follows [11]

$$\theta_c = \frac{1}{s}\omega_c = \frac{1}{s}\overbrace{\left[\left(K_{p,pc} + \frac{K_{i,pc}}{s}\right)\frac{(P_c^\star - P_c)}{S_N} - R_a\frac{P_c}{S_N} + \omega_N\right]}^{G_{pc}}. \tag{3}$$

The control parameters of the APC are tuned using the loop-shaping approach to obtain a first order closed-loop response from $P_c^\star$ to $P_c$. Accordingly, $K_{p,pc} = \frac{\alpha_{pc}}{K_s}S_N$, $K_{i,pc} = \frac{\alpha_{pc}^2}{K_s}S_N$, and $R_a = K_{p,pc}$, with $\alpha_{pc}$ as the loop bandwidth (in rad/s) of the active power controller. The synchronizing power coefficient is given by $K_s = \frac{E_c E_g}{(X_f+\hat{X}_g)}$.

## III. Synchronous Reference Frames Definitions

This section defines the two types of SRFs used to obtain the small-signal models of the grid-connected converter system.

### A. System dq-frame I

The first type of SRF considered here, denoted as the system *dq*-frame I (represented by $d^{\omega_N}$, $q^{\omega_N}$ axes in Fig. 2a) and Fig. 2b)), is defined by the transformation angle, $\theta_N$, which is obtained by integrating $\omega_N$, i.e., $\theta_N = \frac{\omega_N}{s}$. Since the system *dq*-frame I rotates with $\omega_N$, the $d^{\omega_N}$ and $q^{\omega_N}$ axes do not oscillate under small-signal perturbations. On the other hand,

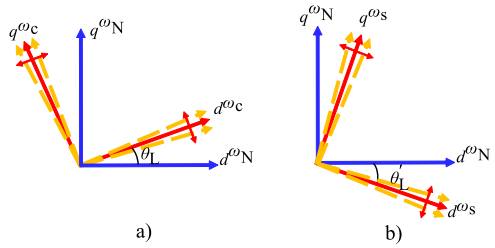


Fig. 2. Representation of a) system *dq*-frame I and converter *dq*-frame, b) system *dq*-frame I and source *dq*-frame under small-signal perturbations.

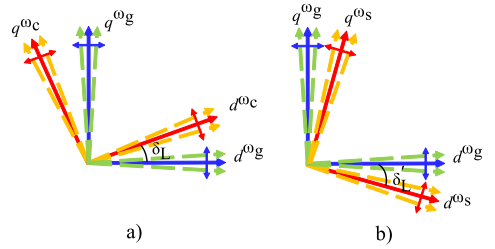


Fig. 3. Representation of a) system *dq*-frame II and converter *dq*-frame, b) system *dq*-frame II and source *dq*-frame under small-signal perturbations.

in accordance with (1) and (3), under small-signal perturbations resulting in power variations, the converter *dq*-frame (rotating with $\omega_c$ and represented by $d^{\omega_c}$, $q^{\omega_c}$ axes in Fig. 2a)) and the source *dq*-frame (rotating with $\omega_s$ and represented by $d^{\omega_s}$, $q^{\omega_s}$ axes in Fig. 2b)), start to oscillate around their respective steady-state positions. The angle difference between the converter *dq*-frame and the system *dq*-frame I is denoted by $\theta_L$ in Fig. 2a), while $\theta'_L$ in Fig. 2b) denotes the angle difference between the system *dq*-frame I and the source *dq*-frame.

### B. System dq-frame II

The second type of SRF considered here, denoted as the system *dq*-frame II (represented by $d^{\omega_g}$ and $q^{\omega_g}$ axes in Fig. 3a) and Fig. 3b)), is aligned to the PCC voltage. Accordingly, it is defined by the PCC voltage angle, $\theta_g$, which is obtained by integrating the fundamental angular frequency, $\omega_g$, of the three-phase voltage at the PCC, i.e., $\theta_g = \frac{\omega_g}{s}$. Unlike the system *dq*-frame I, small-signal perturbations resulting in active power variations (and hence a perturbation in $\omega_g$), causes the $d^{\omega_g}$ and $q^{\omega_g}$ axes to oscillate around their respective steady-state positions, as depicted in Fig. 3a) and Fig. 3b). The angle difference between the converter *dq*-frame and the system *dq*-frame II is denoted by $\delta_L$ in Fig. 3a), while $\delta'_L$ in Fig. 3b) denotes the angle difference between the system *dq*-frame II and the source *dq*-frame.

## IV. Small-Signal Modeling

To analyze small-signal stability of the grid-connected converter system, the overall system is divided into two individual subsystems at the PCC: the converter system and the inertial grid. In this section, small-signal models of these two subsystems are derived analytically and verified using detailed time-domain simulations.

### A. Small-signal model in system dq-frame I

*1) Small-signal modeling of converter system:* To derive the small-signal model of the converter system in the system *dq*-frame I, the controller dynamics described previously should be transformed to this frame. By using (3), the angle $\theta_L$ is given as

$$\theta_L = \theta_c - \theta_N = \frac{1}{s}\frac{[G_{pc}(P_c^\star - P_c) - R_a P_c]}{S_N}. \tag{4}$$

Thus, any space-vector $\underline{z}^{\omega_c}$ defined earlier in the converter *dq*-frame can be transformed to the system *dq*-frame I using the following relation

$$\underline{z}^{\omega_N} = \underline{z}^{\omega_c} e^{j\theta_L}. \tag{5}$$

Using (2), (4) and (5), the small-signal model of the converter voltage reference in the system *dq*-frame I can be expressed as

$$\begin{aligned}\begin{bmatrix}\Delta e_{cd}^{\omega_N\star}\\ \Delta e_{cq}^{\omega_N\star}\end{bmatrix} &= \overbrace{\begin{bmatrix}-(e_{cq0}^{\omega_N} + G_{hpf}R'_a i_{fq0}^{\omega_N}) & G_{vc}\cos\theta_{L0}\\ (e_{cd0}^{\omega_N} + G_{hpf}R'_a i_{fd0}^{\omega_N}) & G_{vc}\sin\theta_{L0}\end{bmatrix}}^{\mathbf{G}_T}\begin{bmatrix}\Delta\theta_L\\ \Delta E_g^\star\end{bmatrix}\\ &+\left(-\overbrace{\begin{bmatrix}\frac{G_{vc}G_{lpf}\cos\theta_{L0}e_{gd0}^{\omega_N}}{E_{g0}} & \frac{G_{vc}G_{lpf}\cos\theta_{L0}e_{gq0}^{\omega_N}}{E_{g0}}\\ \frac{G_{vc}G_{lpf}\sin\theta_{L0}e_{gd0}^{\omega_N}}{E_{g0}} & \frac{G_{vc}G_{lpf}\sin\theta_{L0}e_{gq0}^{\omega_N}}{E_{g0}}\end{bmatrix}}^{\mathbf{G}_{PVv1}}\right)\begin{bmatrix}\Delta e_{gd}^{\omega_N}\\ \Delta e_{gq}^{\omega_N}\end{bmatrix}\\ &+\overbrace{\begin{bmatrix}-G_{hpf}R'_a & 0\\ 0 & -G_{hpf}R'_a\end{bmatrix}}^{\mathbf{G}_{DH}}\begin{bmatrix}\Delta i_{fd}^{\omega_N}\\ \Delta i_{fq}^{\omega_N}\end{bmatrix},\end{aligned} \tag{6}$$

with

$$\begin{bmatrix}\Delta\theta_L\\ \Delta E_g^\star\end{bmatrix} = \begin{bmatrix}\frac{G_{pc}}{sS_N} & 0\\ 0 & 1\end{bmatrix}\begin{bmatrix}\Delta P_c^\star\\ \Delta E_g^\star\end{bmatrix}$$

$$+\overbrace{\begin{bmatrix}-\frac{(G_{pc}+R_a)e_{gd0}^{\omega_N}}{sS_N} & -\frac{(G_{pc}+R_a)e_{gq0}^{\omega_N}}{sS_N}\\ 0 & 0\end{bmatrix}}^{\mathbf{G}_{PVc2}}\begin{bmatrix}\Delta i_{fd}^{\omega_N}\\ \Delta i_{fq}^{\omega_N}\end{bmatrix} \tag{7}$$

$$+\overbrace{\begin{bmatrix}-\frac{(G_{pc}+R_a)i_{fd0}^{\omega_N}}{sS_N} & -\frac{(G_{pc}+R_a)i_{fq0}^{\omega_N}}{sS_N}\\ 0 & 0\end{bmatrix}}^{\mathbf{G}_{PVv2}}\begin{bmatrix}\Delta e_{gd}^{\omega_N}\\ \Delta e_{gq}^{\omega_N}\end{bmatrix},$$

where the expressions $P_c = e_{gd}^{\omega_N} i_{fd}^{\omega_N} + e_{gq}^{\omega_N} i_{fq}^{\omega_N}$, and $E_g = \sqrt{(e_{gd}^{\omega_N})^2 + (e_{gq}^{\omega_N})^2}$ are used for the active power output of the converter and the PCC-voltage magnitude, respectively. The subscript "0" represents steady-state quantities in the notations. By neglecting the impact of delays and using (6), (7) and the linearized expression for the current dynamics in the system *dq*-frame I, which is given by

$$\begin{bmatrix}\Delta e_{cd}^{\omega_N}\\ \Delta e_{cq}^{\omega_N}\end{bmatrix} = \begin{bmatrix}\Delta e_{gd}^{\omega_N}\\ \Delta e_{gq}^{\omega_N}\end{bmatrix} + \overbrace{\begin{bmatrix}R_f + sL_f & -\omega_N L_f\\ \omega_N L_f & R_f + sL_f\end{bmatrix}}^{\mathbf{Z}_f}\begin{bmatrix}\Delta i_{fd}^{\omega_N}\\ \Delta i_{fq}^{\omega_N}\end{bmatrix}, \tag{8}$$

the small-signal model of the converter system in the system *dq*-frame I can be obtained in its conventional form as

$$\overbrace{\begin{bmatrix}\Delta i_{fd}^{\omega_N}\\ \Delta i_{fq}^{\omega_N}\end{bmatrix}}^{\mathbf{I}_f} = \mathbf{G}_c\begin{bmatrix}\Delta P_c^\star\\ \Delta E_g^\star\end{bmatrix} - \mathbf{Y}_c\overbrace{\begin{bmatrix}\Delta e_{gd}^{\omega_N}\\ \Delta e_{gq}^{\omega_N}\end{bmatrix}}^{\mathbf{E}_g}, \tag{9}$$

where $\mathbf{Y}_{\rm c}$ denotes the input-admittance[2] of the converter system seen from the PCC and is given by

$$\mathbf{Y}_{\rm c} = [\mathbf{G}_{\rm T}\mathbf{G}_{\rm PVc2} + \mathbf{G}_{\rm DH} - \mathbf{Z}_{\rm f}]^{-1}[\mathbf{G}_{\rm T}\mathbf{G}_{\rm PVv2} - \mathbf{G}_{\rm PVv1} - \mathbf{I}], \tag{10}$$

with $\mathbf{I}$ denoting the identity matrix of dimension 2×2.

To obtain the small-signal model of the converter system based on variations in the magnitude and frequency of the PCC voltage, a transfer matrix relating variations in the $dq$-components of the PCC voltage in system $dq$-frame I with variations in the magnitude and frequency of the PCC voltage is derived. Considering the PCC voltage vector in the stationary $\alpha\beta$-frame, which is given as

$$\underline{e}_{\rm g}^{\alpha\beta} = E_{\rm g}e^{j\theta_{\rm g}}, \tag{11}$$

the PCC voltage vector in the system $dq$-frame I can be obtained as

$$\underline{e}_{\rm g}^{\omega_{\rm N}} = E_{\rm g}e^{j(\theta_{\rm g}-\theta_{\rm N})}. \tag{12}$$

During a small perturbation resulting in variation of both voltage magnitude and fundamental frequency at the PCC (hence a variation in $\theta_{\rm g}$), the variation in $\underline{e}_{\rm g}^{\omega_{\rm N}}$ can be obtained by linearizing (12) as

$$\Delta\underline{e}_{\rm g}^{\omega_{\rm N}} = jE_{\rm g0}e^{j(\theta_{\rm g0}-\theta_{\rm N0})}\Delta\theta_{\rm g} + e^{j(\theta_{\rm g0}-\theta_{\rm N0})}\Delta E_{\rm g}. \tag{13}$$

If the system $dq$-frame I is aligned so that the $d^{\omega_{\rm N}}$-axis coincides with the PCC voltage vector in steady-state, i.e., $\theta_{\rm g0} = \theta_{\rm N0}$, expression (13) can be simplified as

$$\Delta\underline{e}_{\rm g}^{\omega_{\rm N}} = jE_{\rm g0}\frac{\Delta\omega_{\rm g}}{s} + \Delta E_{\rm g}. \tag{14}$$

Equation (14) can be expressed in its components form as

$$\begin{bmatrix}\Delta e_{\rm gd}^{\omega_{\rm N}}\\ \Delta e_{\rm gq}^{\omega_{\rm N}}\end{bmatrix} = \begin{bmatrix}1 & 0\\ 0 & \frac{E_{\rm g0}}{s}\end{bmatrix}\begin{bmatrix}\Delta E_{\rm g}\\ \Delta\omega_{\rm g}\end{bmatrix}. \tag{15}$$

By substituting expression (15) in (9) and for the case where reference values for the active power and PCC-voltage magnitude remain constant (implying that $\Delta P_{\rm c}^{\star} = \Delta E_{\rm g}^{\star} = 0$), the small-signal model of the converter system based on voltage magnitude and frequency perturbations at the PCC can be obtained in the system $dq$-frame I as

$$\begin{bmatrix}\Delta i_{\rm fd}^{\omega_{\rm N}}\\ \Delta i_{\rm fq}^{\omega_{\rm N}}\end{bmatrix} = -\begin{bmatrix}Y_{\rm c}(1,1) & Y_{\rm c}(1,2)\frac{E_{\rm g0}}{s}\\ Y_{\rm c}(2,1) & Y_{\rm c}(2,2)\frac{E_{\rm g0}}{s}\end{bmatrix}\begin{bmatrix}\Delta E_{\rm g}\\ \Delta\omega_{\rm g}\end{bmatrix}. \tag{16}$$

Finally, by utilizing (15), (16) and expressions for active and reactive power output of the converter, i.e., $P_{\rm c} = e_{\rm gd}^{\omega_{\rm N}}i_{\rm fd}^{\omega_{\rm N}} + e_{\rm gq}^{\omega_{\rm N}}i_{\rm fq}^{\omega_{\rm N}}$, and $Q_{\rm c} = -e_{\rm gd}^{\omega_{\rm N}}i_{\rm fq}^{\omega_{\rm N}} + e_{\rm gq}^{\omega_{\rm N}}i_{\rm fd}^{\omega_{\rm N}}$, the small-signal model of the converter system can be expressed in terms of its active and reactive power variations as

$$\overbrace{\begin{bmatrix}\Delta P_{\rm c}\\ \Delta Q_{\rm c}\end{bmatrix}}^{\mathbf{S}_{\rm c}} = -\overbrace{\begin{bmatrix}E_{\rm g0}Y_{\rm c}(1,1) - i_{\rm fd0}^{\omega_{\rm N}} & \frac{E_{\rm g0}^2Y_{\rm c}(1,2) - i_{\rm fq0}^{\omega_{\rm N}}E_{\rm g0}}{s}\\ -E_{\rm g0}Y_{\rm c}(2,1) + i_{\rm fq0}^{\omega_{\rm N}} & \frac{-E_{\rm g0}^2Y_{\rm c}(2,2) - i_{\rm fd0}^{\omega_{\rm N}}E_{\rm g0}}{s}\end{bmatrix}}^{\mathbf{G}_{\rm tmc}}\overbrace{\begin{bmatrix}\Delta E_{\rm g}\\ \Delta\omega_{\rm g}\end{bmatrix}}^{\mathbf{E}_{\Omega}}. \tag{17}$$

[2]Since the direction of current flowing out of the converter in Fig. 1 is taken as positive, the negative sign for $\mathbf{Y}_{\rm c}$ is used in (9).

It can be inferred from (17) that the elements of the converter's power-response matrix, $\mathbf{G}_{\rm tmc}$, provide direct insight into the services offered by the converter system when subjected to grid disturbances. For instance, the frequency characteristic of the (1,2) element of $\mathbf{G}_{\rm tmc}$, which relates perturbation in the fundamental angular frequency of the PCC voltage to variation in the active power of the converter system[3], can be used to assess the frequency-droop and inertial behaviors of the converter system, along with its damping properties. Similarly, frequency response of the (2,1) element of $\mathbf{G}_{\rm tmc}$ can be used for assessing voltage-droop behavior of the converter system.

*2) Small-signal modeling of inertial grid:* To derive the small-signal model of the inertial grid, the source voltage vector, $\underline{e}_{\rm s}^{\omega_{\rm s}}$, in the source $dq$-frame (defined by the transformation angle, $\theta_{\rm s}$, which is obtained by integrating the angular frequency of the voltage source, i.e., $\theta_{\rm s} = \frac{\omega_{\rm s}}{s}$) should be transformed to the system $dq$-frame I. By using the swing equation in (1), this transformation can be achieved from the following expression

$$\underline{e}_{\rm s}^{\omega_{\rm N}} = \underline{e}_{\rm s}^{\omega_{\rm s}}e^{-j\theta_{\rm L}'}, \quad \text{with} \quad \theta_{\rm L}' = \theta_{\rm N} - \theta_{\rm s} = \frac{1}{s}\frac{G_{\rm pc}'(P_{\rm g}^{\star} - P_{\rm g})}{S_{\rm N}}. \tag{18}$$

Linearizing (18), the small-signal model of the source voltage vector in the system $dq$-frame I can be expressed as

$$\begin{bmatrix}\Delta e_{\rm sd}^{\omega_{\rm N}}\\ \Delta e_{\rm sq}^{\omega_{\rm N}}\end{bmatrix} = \overbrace{\begin{bmatrix}e_{\rm sq0}^{\omega_{\rm N}} & 0\\ -e_{\rm sd0}^{\omega_{\rm N}} & 0\end{bmatrix}}^{\mathbf{G}_{e\theta}}\begin{bmatrix}\Delta\theta_{\rm L}'\\ 0\end{bmatrix} + \overbrace{\begin{bmatrix}\cos\theta_{\rm L0}' & \sin\theta_{\rm L0}'\\ -\sin\theta_{\rm L0}' & \cos\theta_{\rm L0}'\end{bmatrix}}^{\mathbf{G}_{\rm te}}\begin{bmatrix}\Delta e_{\rm sd}^{\omega_{\rm s}}\\ \Delta e_{\rm sq}^{\omega_{\rm s}}\end{bmatrix}, \tag{19}$$

with

$$\begin{bmatrix}\Delta\theta_{\rm L}'\\ 0\end{bmatrix} = \begin{bmatrix}\frac{G_{\rm pc}'}{sS_{\rm N}} & 0\\ 0 & 1\end{bmatrix}\begin{bmatrix}\Delta P_{\rm g}^{\star}\\ 0\end{bmatrix} + \overbrace{\begin{bmatrix}-\frac{G_{\rm pc}'e_{\rm gd0}^{\omega_{\rm N}}}{sS_{\rm N}} & -\frac{G_{\rm pc}'e_{\rm gq0}^{\omega_{\rm N}}}{sS_{\rm N}}\\ 0 & 0\end{bmatrix}}^{\mathbf{G}_{\theta{\rm i}}}\begin{bmatrix}\Delta i_{\rm gd}^{\omega_{\rm N}}\\ \Delta i_{\rm gq}^{\omega_{\rm N}}\end{bmatrix} + \overbrace{\begin{bmatrix}-\frac{G_{\rm pc}'i_{\rm gd0}^{\omega_{\rm N}}}{sS_{\rm N}} & -\frac{G_{\rm pc}'i_{\rm gq0}^{\omega_{\rm N}}}{sS_{\rm N}}\\ 0 & 0\end{bmatrix}}^{\mathbf{G}_{\theta{\rm e}}}\begin{bmatrix}\Delta e_{\rm gd}^{\omega_{\rm N}}\\ \Delta e_{\rm gq}^{\omega_{\rm N}}\end{bmatrix}, \tag{20}$$

where the expression $P_{\rm g} = e_{\rm gd}^{\omega_{\rm N}}i_{\rm gd}^{\omega_{\rm N}} + e_{\rm gq}^{\omega_{\rm N}}i_{\rm gq}^{\omega_{\rm N}}$ is used for the active power injected into the grid. Since the magnitude of the source voltage is assumed constant, $\Delta e_{\rm sd}^{\omega_{\rm s}} = \Delta e_{\rm sq}^{\omega_{\rm s}} = 0$. By substituting (20) in (19) and using the linearized expression for the current dynamics in the system $dq$-frame I, which is given by

$$\begin{bmatrix}\Delta e_{\rm sd}^{\omega_{\rm N}}\\ \Delta e_{\rm sq}^{\omega_{\rm N}}\end{bmatrix} = \begin{bmatrix}\Delta e_{\rm gd}^{\omega_{\rm N}}\\ \Delta e_{\rm gq}^{\omega_{\rm N}}\end{bmatrix} - \overbrace{\begin{bmatrix}R_{\rm g} + sL_{\rm g} & -\omega_{\rm N}L_{\rm g}\\ \omega_{\rm N}L_{\rm g} & R_{\rm g} + sL_{\rm g}\end{bmatrix}}^{\mathbf{Z}_{\rm g}}\begin{bmatrix}\Delta i_{\rm gd}^{\omega_{\rm N}}\\ \Delta i_{\rm gq}^{\omega_{\rm N}}\end{bmatrix}, \tag{21}$$

the small-signal model of the inertial grid in the system $dq$-frame I can be obtained in its conventional form as

$$\overbrace{\begin{bmatrix}\Delta i_{\rm gd}^{\omega_{\rm N}}\\ \Delta i_{\rm gq}^{\omega_{\rm N}}\end{bmatrix}}^{\mathbf{I}_{\rm g}} = \mathbf{G}_{\rm g}\begin{bmatrix}\Delta P_{\rm g}^{\star}\\ 0\end{bmatrix} + \mathbf{Y}_{\rm g}\overbrace{\begin{bmatrix}\Delta e_{\rm gd}^{\omega_{\rm N}}\\ \Delta e_{\rm gq}^{\omega_{\rm N}}\end{bmatrix}}^{\mathbf{E}_{\rm g}}, \tag{22}$$

[3]Also referred to as the network frequency perturbation response [9], [10] of the converter system

TABLE I
SYSTEM AND CONTROL PARAMETERS FOR CONSIDERED SYSTEM

| System parameters | | Control parameters | |
|---|---|---|---|
| $S_{\rm N}$ | 100 MVA (1.0 pu) | $H$ | 5 s |
| $E_{\rm N}$ | 20 kV (1.0 pu) | $K_{\rm D}$ | 50 pu |
| $\omega_{\rm N}$ | 314.16 rad/s (1.0 pu) | $\alpha_{\rm vc}$ | $2\pi 1$ rad/s |
| $R_{\rm f}$ | 0.015 pu | $\alpha_{\rm hpf}$ | $2\pi 5$ rad/s |
| $L_{\rm f}$ | 0.15 pu | $R'_{\rm a}$ | 0.1 pu |
| $R_{\rm g}$ | 0.02 pu | $\alpha_{\rm lpf}$ | $2\pi 100$ rad/s |
| $L_{\rm g}$ | 0.2 pu | $\alpha_{\rm pc}$ | $2\pi 5$ rad/s |

where $\mathbf{Y}_{\rm g}$ denotes the input-admittance of the inertial grid seen from the PCC and is given by

$$\mathbf{Y}_{\rm g} = [\mathbf{G}_{{\rm e}\theta}\mathbf{G}_{\theta{\rm i}} + \mathbf{Z}_{\rm g}]^{-1}[\mathbf{I} - \mathbf{G}_{{\rm e}\theta}\mathbf{G}_{\theta{\rm e}}]. \tag{23}$$

By using a similar approach as the one described for the converter system in the previous sub-section, the small-signal model of the inertial grid based on voltage magnitude and frequency perturbations at the PCC can be obtained in the system $dq$-frame I as

$$\begin{bmatrix}\Delta i_{\rm gd}^{\omega_{\rm N}} \\ \Delta i_{\rm gq}^{\omega_{\rm N}}\end{bmatrix} = \begin{bmatrix} Y_{\rm g}(1,1) & Y_{\rm g}(1,2)\frac{E_{\rm g0}}{s} \\ Y_{\rm g}(2,1) & Y_{\rm g}(2,2)\frac{E_{\rm g0}}{s}\end{bmatrix}\begin{bmatrix}\Delta E_{\rm g} \\ \Delta\omega_{\rm g}\end{bmatrix}. \tag{24}$$

Finally, by utilizing (15), (24) and expressions for active and reactive power injected to the grid, i.e., $P_{\rm g} = e_{\rm gd}^{\omega_{\rm N}} i_{\rm gd}^{\omega_{\rm N}} + e_{\rm gq}^{\omega_{\rm N}} i_{\rm gq}^{\omega_{\rm N}}$, and $Q_{\rm g} = -e_{\rm gd}^{\omega_{\rm N}} i_{\rm gq}^{\omega_{\rm N}} + e_{\rm gq}^{\omega_{\rm N}} i_{\rm gd}^{\omega_{\rm N}}$, the small-signal model of the inertial grid can be expressed in terms of its active and reactive power variations as

$$\overbrace{\begin{bmatrix}\Delta P_{\rm g} \\ \Delta Q_{\rm g}\end{bmatrix}}^{\mathbf{S}_{\rm g}} = \overbrace{\begin{bmatrix} E_{\rm g0}Y_{\rm g}(1,1) + i_{\rm gd0}^{\omega_{\rm N}} & \frac{E_{\rm g0}^2 Y_{\rm g}(1,2) + i_{\rm gq0}^{\omega_{\rm N}} E_{\rm g0}}{s} \\ -E_{\rm g0}Y_{\rm g}(2,1) - i_{\rm gq0}^{\omega_{\rm N}} & \frac{-E_{\rm g0}^2 Y_{\rm g}(2,2) + i_{\rm gd0}^{\omega_{\rm N}} E_{\rm g0}}{s}\end{bmatrix}}^{\mathbf{G}_{\rm tmg}} \overbrace{\begin{bmatrix}\Delta E_{\rm g} \\ \Delta\omega_{\rm g}\end{bmatrix}}^{\mathbf{E}_\Omega}. \tag{25}$$

*3) Verification of derived small-signal models:* To verify the analytically derived power-response matrices of the converter system ($\mathbf{G}_{\rm tmc}$) and the inertial grid ($\mathbf{G}_{\rm tmg}$), detailed PSCAD/EMTDC time-domain simulation of the grid-connected converter system shown in Fig. 1 including all control loops (implemented in discrete time) is used. Independent perturbations in the voltage magnitude and frequency are applied at the PCC to the individual subsystems at various frequencies. For each perturbation, the resulting perturbations in the active and reactive power of the respective subsystem are measured, and the power-response matrix of each subsystem is extracted using Discrete Fourier Transform (DFT) calculations.

For all the simulations tests performed in this manuscript, system and control parameters stated in Table I are used unless stated explicitly. Furthermore, the simulation tests are performed with the converter system injecting 0.8 pu active power and regulating the PCC voltage to 1.0 pu. Figures 4 and 5 show the frequency response of the real and imaginary parts of the first row elements of $\mathbf{G}_{\rm tmc}$ and $\mathbf{G}_{\rm tmg}$, respectively. Due to space constraints, the second row elements are not shown here. The results demonstrate a very good match between the analytical frequency characteristics and those obtained from simulations, verifying the validity of the analytical models.

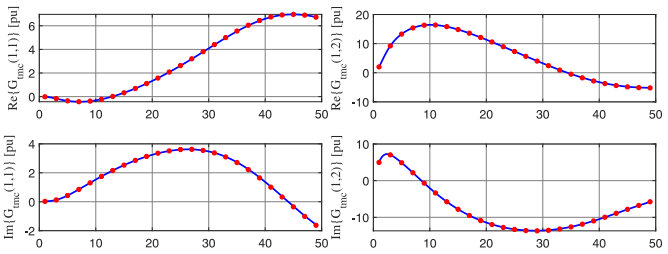


Fig. 4. Frequency response of the first row elements of $\mathbf{G}_{\rm tmc}$; analytical model (solid-blue curves) and simulation model (dotted-red curves).

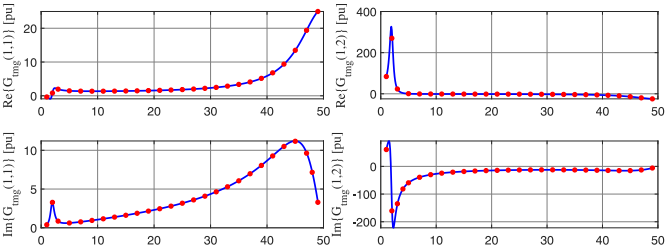


Fig. 5. Frequency response of the first row elements of $\mathbf{G}_{\rm tmg}$; analytical model (solid-blue curves) and simulation model (dotted-red curves).

## B. Small-signal model in system dq-frame II

*1) Small-signal modeling of converter system:* To derive the small-signal model of the converter system in the system $dq$-frame II, the controller dynamics should be transformed to this frame using the following relation

$$\underline{z}^{\omega_{\rm g}} = \underline{z}^{\omega_{\rm c}} e^{j\delta_{\rm L}}, \quad \text{with} \quad \delta_{\rm L} = \theta_{\rm c} - \theta_{\rm g}. \tag{26}$$

Using (2), (3) and (26), the small-signal model of the converter voltage reference in the system $dq$-frame II can be expressed as

$$\begin{aligned}\begin{bmatrix}\Delta e_{\rm cd}^{\omega_{\rm g}\star} \\ \Delta e_{\rm cq}^{\omega_{\rm g}\star}\end{bmatrix} &= \overbrace{\begin{bmatrix} -(e_{\rm cq0}^{\omega_{\rm g}} + G_{\rm hpf}R'_{\rm a}i_{\rm fq0}^{\omega_{\rm g}}) & G'_{\rm vc}\cos\delta_{\rm L0} \\ (e_{\rm cd0}^{\omega_{\rm g}} + G_{\rm hpf}R'_{\rm a}i_{\rm fd0}^{\omega_{\rm g}}) & G'_{\rm vc}\sin\delta_{\rm L0}\end{bmatrix}}^{\mathbf{G}'_{\rm T}}\begin{bmatrix}\Delta\delta_{\rm L} \\ \Delta E_{\rm g}^\star\end{bmatrix} \\ &+ \left(-\overbrace{\begin{bmatrix}\frac{G_{\rm vc}G_{\rm lpf}\cos\delta_{\rm L0}e_{\rm gd0}^{\omega_{\rm g}}}{E_{\rm g0}} & \frac{G_{\rm vc}G_{\rm lpf}\cos\delta_{\rm L0}e_{\rm gq0}^{\omega_{\rm g}}}{E_{\rm g0}} \\ \frac{G_{\rm vc}G_{\rm lpf}\sin\delta_{\rm L0}e_{\rm gd0}^{\omega_{\rm g}}}{E_{\rm g0}} & \frac{G_{\rm vc}G_{\rm lpf}\sin\delta_{\rm L0}e_{\rm gq0}^{\omega_{\rm g}}}{E_{\rm g0}}\end{bmatrix}}^{\mathbf{G}'_{\rm PVv1}}\right)\begin{bmatrix}\Delta e_{\rm gd}^{\omega_{\rm g}} \\ \Delta e_{\rm gq}^{\omega_{\rm g}}\end{bmatrix} \\ &+ \overbrace{\begin{bmatrix}-G_{\rm hpf}R'_{\rm a} & 0 \\ 0 & -G_{\rm hpf}R'_{\rm a}\end{bmatrix}}^{\mathbf{G}'_{\rm DH}}\begin{bmatrix}\Delta i_{\rm fd}^{\omega_{\rm g}} \\ \Delta i_{\rm fq}^{\omega_{\rm g}}\end{bmatrix},\end{aligned} \tag{27}$$

with

$$\begin{aligned}\begin{bmatrix}\Delta\delta_{\rm L} \\ \Delta E_{\rm g}^\star\end{bmatrix} &= \begin{bmatrix}\frac{G_{\rm pc}}{sS_{\rm N}} & 0 \\ 0 & 1\end{bmatrix}\begin{bmatrix}\Delta P_{\rm c}^\star \\ \Delta E_{\rm g}^\star\end{bmatrix} \\ &+ \overbrace{\begin{bmatrix}-\frac{(G_{\rm pc}+R_{\rm a})e_{\rm gd0}^{\omega_{\rm g}}}{sS_{\rm N}} & -\frac{(G_{\rm pc}+R_{\rm a})e_{\rm gq0}^{\omega_{\rm g}}}{sS_{\rm N}} \\ 0 & 0\end{bmatrix}}^{\mathbf{G}'_{\rm PVc2}}\begin{bmatrix}\Delta i_{\rm fd}^{\omega_{\rm g}} \\ \Delta i_{\rm fq}^{\omega_{\rm g}}\end{bmatrix} \\ &+ \overbrace{\begin{bmatrix}-\frac{(G_{\rm pc}+R_{\rm a})i_{\rm fd0}^{\omega_{\rm g}}}{sS_{\rm N}} & -\frac{(G_{\rm pc}+R_{\rm a})i_{\rm fq0}^{\omega_{\rm g}}}{sS_{\rm N}} \\ 0 & 0\end{bmatrix}}^{\mathbf{G}'_{\rm PVv2}}\begin{bmatrix}\Delta e_{\rm gd}^{\omega_{\rm g}} \\ \Delta e_{\rm gq}^{\omega_{\rm g}}\end{bmatrix} - \overbrace{\begin{bmatrix}\frac{1}{s} & 0 \\ 0 & 0\end{bmatrix}}^{\mathbf{G}'_{\delta\omega}}\begin{bmatrix}\Delta\omega_{\rm g} \\ 0\end{bmatrix},\end{aligned} \tag{28}$$

where the expressions $P_{\rm c} = e_{\rm gd}^{\omega_{\rm g}} i_{\rm fd}^{\omega_{\rm g}} + e_{\rm gq}^{\omega_{\rm g}} i_{\rm fq}^{\omega_{\rm g}}$, and $E_{\rm g} = \sqrt{(e_{\rm gd}^{\omega_{\rm g}})^2 + (e_{\rm gq}^{\omega_{\rm g}})^2}$ are used for the active power output of the converter and the PCC-voltage magnitude, respectively.

Again, by neglecting the impact of delays and using (27), (28) and the linearized expression for the current dynamics in the system *dq*-frame II, which is given by

$$\begin{bmatrix}\Delta e_{\rm cd}^{\omega_{\rm g}}\\ \Delta e_{\rm cq}^{\omega_{\rm g}}\end{bmatrix} = \begin{bmatrix}\Delta e_{\rm gd}^{\omega_{\rm g}}\\ \Delta e_{\rm gq}^{\omega_{\rm g}}\end{bmatrix} + \overbrace{\begin{bmatrix}R_{\rm f}+sL_{\rm f} & -\omega_{\rm N}L_{\rm f}\\ \omega_{\rm N}L_{\rm f} & R_{\rm f}+sL_{\rm f}\end{bmatrix}}^{\mathbf{Z}'_{\rm f}} \begin{bmatrix}\Delta i_{\rm fd}^{\omega_{\rm g}}\\ \Delta i_{\rm fq}^{\omega_{\rm g}}\end{bmatrix} + \overbrace{\begin{bmatrix}-L_{\rm f} i_{\rm fq0}^{\omega_{\rm g}} & 0\\ L_{\rm f} i_{\rm fd0}^{\omega_{\rm g}} & 0\end{bmatrix}}^{\mathbf{G}'_{\rm v\omega}} \begin{bmatrix}\Delta\omega_{\rm g}\\ 0\end{bmatrix}, \tag{29}$$

the small-signal model of the converter system in the system *dq*-frame II is derived as

$$\begin{bmatrix}\Delta i_{\rm fd}^{\omega_{\rm g}}\\ \Delta i_{\rm fq}^{\omega_{\rm g}}\end{bmatrix} = \mathbf{G}'_{\rm c}\begin{bmatrix}\Delta P_{\rm c}^{\star}\\ \Delta E_{\rm g}^{\star}\end{bmatrix} - \mathbf{Y}'_{\rm c}\begin{bmatrix}\Delta e_{\rm gd}^{\omega_{\rm g}}\\ \Delta e_{\rm gq}^{\omega_{\rm g}}\end{bmatrix} - \mathbf{G}'_{\rm ic\omega}\begin{bmatrix}\Delta\omega_{\rm g}\\ 0\end{bmatrix}, \tag{30}$$

where $\mathbf{Y}'_{\rm c}$ and $\mathbf{G}'_{\rm ic\omega}$ are given by

$$\mathbf{Y}'_{\rm c} = [\mathbf{G}'_{\rm T}\mathbf{G}'_{\rm PVc2} + \mathbf{G}'_{\rm DH} - \mathbf{Z}'_{\rm f}]^{-1}[\mathbf{G}'_{\rm T}\mathbf{G}'_{\rm PVv2} - \mathbf{G}'_{\rm PVv1} - \mathbf{I}], \tag{31}$$

$$\mathbf{G}'_{\rm ic\omega} = -[\mathbf{G}'_{\rm T}\mathbf{G}'_{\rm PVc2} + \mathbf{G}'_{\rm DH} - \mathbf{Z}'_{\rm f}]^{-1}[\mathbf{G}'_{\rm v\omega} + \mathbf{G}'_{\rm T}\mathbf{G}'_{\delta\omega}]. \tag{32}$$

Since the system *dq*-frame II is aligned to the PCC voltage, variations in the magnitude of the PCC voltage are only reflected in terms of variations in the *d*-component of the voltage in this frame, i.e., $\Delta e_{\rm gd}^{\omega_{\rm g}} = \Delta E_{\rm g}$ and $\Delta e_{\rm gq}^{\omega_{\rm g}} = 0$. Furthermore, the current dynamics in the converter resulting from frequency variations at the PCC can be obtained using the transfer matrix $\mathbf{G}'_{\rm ic\omega}$. Accordingly, for the case where reference values for the active power and PCC-voltage magnitude remain constant, the small-signal model of the converter system based on voltage magnitude and frequency perturbations at the PCC can be obtained in the system *dq*-frame II as

$$\begin{bmatrix}\Delta i_{\rm fd}^{\omega_{\rm g}}\\ \Delta i_{\rm fq}^{\omega_{\rm g}}\end{bmatrix} = -\begin{bmatrix}Y'_{\rm c}(1,1) & G'_{\rm ic\omega}(1,1)\\ Y'_{\rm c}(2,1) & G'_{\rm ic\omega}(2,1)\end{bmatrix}\begin{bmatrix}\Delta E_{\rm g}\\ \Delta\omega_{\rm g}\end{bmatrix}. \tag{33}$$

Finally, by utilizing (33) and expressions for active and reactive power output of the converter, i.e., $P_{\rm c} = e_{\rm gd}^{\omega_{\rm g}} i_{\rm fd}^{\omega_{\rm g}} + e_{\rm gq}^{\omega_{\rm g}} i_{\rm fq}^{\omega_{\rm g}}$, and $Q_{\rm c} = -e_{\rm gd}^{\omega_{\rm g}} i_{\rm fq}^{\omega_{\rm g}} + e_{\rm gq}^{\omega_{\rm g}} i_{\rm fd}^{\omega_{\rm g}}$, the small-signal model of the converter system in terms of its active and reactive power variations can be obtained as

$$\begin{bmatrix}\Delta P_{\rm c}\\ \Delta Q_{\rm c}\end{bmatrix} = -\overbrace{\begin{bmatrix}E_{\rm g0}Y'_{\rm c}(1,1) - i_{\rm fd0}^{\omega_{\rm g}} & E_{\rm g0}G'_{\rm ic\omega}(1,1)\\ -E_{\rm g0}Y'_{\rm c}(2,1) + i_{\rm fq0}^{\omega_{\rm g}} & -E_{\rm g0}G'_{\rm ic\omega}(2,1)\end{bmatrix}}^{\mathbf{G}'_{\rm tmc}}\begin{bmatrix}\Delta E_{\rm g}\\ \Delta\omega_{\rm g}\end{bmatrix}. \tag{34}$$

*2) Small-signal modeling of inertial grid:* To derive the small-signal model of the inertial grid, the source voltage vector in the source *dq*-frame should be transformed to the system *dq*-frame II using the following expression

$$\underline{e}_{\rm s}^{\omega_{\rm g}} = \underline{e}_{\rm s}^{\omega_{\rm s}} e^{-j\delta'_{\rm L}}, \quad \text{with} \quad \delta'_{\rm L} = \theta_{\rm g} - \theta_{\rm s}. \tag{35}$$

Linearizing (1) and (35), the small-signal model of the source voltage vector in the system *dq*-frame II can be expressed in its components form as

$$\begin{bmatrix}\Delta e_{\rm sd}^{\omega_{\rm g}}\\ \Delta e_{\rm sq}^{\omega_{\rm g}}\end{bmatrix} = \overbrace{\begin{bmatrix}e_{\rm sq0}^{\omega_{\rm g}} & 0\\ -e_{\rm sd0}^{\omega_{\rm g}} & 0\end{bmatrix}}^{\mathbf{G}'_{e\theta}}\begin{bmatrix}\Delta\delta'_{\rm L}\\ 0\end{bmatrix} + \overbrace{\begin{bmatrix}\cos\delta'_{\rm L0} & \sin\delta'_{\rm L0}\\ -\sin\delta'_{\rm L0} & \cos\delta'_{\rm L0}\end{bmatrix}}^{\mathbf{G}'_{\rm te}}\begin{bmatrix}\Delta e_{\rm sd}^{\omega_{\rm s}}\\ \Delta e_{\rm sq}^{\omega_{\rm s}}\end{bmatrix}, \tag{36}$$

with

$$\begin{aligned}\begin{bmatrix}\Delta\delta'_{\rm L}\\ 0\end{bmatrix} &= \overbrace{\begin{bmatrix}\frac{1}{s} & 0\\ 0 & 0\end{bmatrix}}^{\mathbf{G}'_{\delta\omega}}\begin{bmatrix}\Delta\omega_{\rm g}\\ 0\end{bmatrix} + \begin{bmatrix}\frac{G'_{\rm pc}}{sS_{\rm N}} & 0\\ 0 & 1\end{bmatrix}\begin{bmatrix}\Delta P_{\rm g}^{\star}\\ 0\end{bmatrix}\\ &+ \overbrace{\begin{bmatrix}-\frac{G'_{\rm pc}e_{\rm gd0}^{\omega_{\rm g}}}{sS_{\rm N}} & -\frac{G'_{\rm pc}e_{\rm gq0}^{\omega_{\rm g}}}{sS_{\rm N}}\\ 0 & 0\end{bmatrix}}^{\mathbf{G}'_{\theta\rm i}}\begin{bmatrix}\Delta i_{\rm gd}^{\omega_{\rm g}}\\ \Delta i_{\rm gq}^{\omega_{\rm g}}\end{bmatrix}\\ &+ \overbrace{\begin{bmatrix}-\frac{G'_{\rm pc}i_{\rm gd0}^{\omega_{\rm g}}}{sS_{\rm N}} & -\frac{G'_{\rm pc}i_{\rm gq0}^{\omega_{\rm g}}}{sS_{\rm N}}\\ 0 & 0\end{bmatrix}}^{\mathbf{G}'_{\theta\rm e}}\begin{bmatrix}\Delta e_{\rm gd}^{\omega_{\rm g}}\\ \Delta e_{\rm gq}^{\omega_{\rm g}}\end{bmatrix},\end{aligned} \tag{37}$$

where the expression $P_{\rm g} = e_{\rm gd}^{\omega_{\rm g}} i_{\rm gd}^{\omega_{\rm g}} + e_{\rm gq}^{\omega_{\rm g}} i_{\rm gq}^{\omega_{\rm g}}$ is used for the active power injected into the grid. Since the magnitude of the source voltage is assumed constant, $\Delta e_{\rm sd}^{\omega_{\rm s}} = \Delta e_{\rm sq}^{\omega_{\rm s}} = 0$. Finally, by substituting (37) in (36) and using the linearized expression for the current dynamics in the system *dq*-frame II, which is given by

$$\begin{bmatrix}\Delta e_{\rm sd}^{\omega_{\rm g}}\\ \Delta e_{\rm sq}^{\omega_{\rm g}}\end{bmatrix} = \begin{bmatrix}\Delta e_{\rm gd}^{\omega_{\rm g}}\\ \Delta e_{\rm gq}^{\omega_{\rm g}}\end{bmatrix} - \overbrace{\begin{bmatrix}R_{\rm g}+sL_{\rm g} & -\omega_{\rm N}L_{\rm g}\\ \omega_{\rm N}L_{\rm g} & R_{\rm g}+sL_{\rm g}\end{bmatrix}}^{\mathbf{Z}'_{\rm g}}\begin{bmatrix}\Delta i_{\rm gd}^{\omega_{\rm g}}\\ \Delta i_{\rm gq}^{\omega_{\rm g}}\end{bmatrix} - \overbrace{\begin{bmatrix}-L_{\rm g} i_{\rm gq0}^{\omega_{\rm g}} & 0\\ L_{\rm g} i_{\rm gd0}^{\omega_{\rm g}} & 0\end{bmatrix}}^{\mathbf{G}'_{e\omega}}\begin{bmatrix}\Delta\omega_{\rm g}\\ 0\end{bmatrix}, \tag{38}$$

the small-signal model of the inertial grid in the system *dq*-frame II is derived as

$$\begin{bmatrix}\Delta i_{\rm gd}^{\omega_{\rm g}}\\ \Delta i_{\rm gq}^{\omega_{\rm g}}\end{bmatrix} = \mathbf{G}'_{\rm g}\begin{bmatrix}\Delta P^{\star}\\ 0\end{bmatrix} + \mathbf{Y}'_{\rm g}\begin{bmatrix}\Delta e_{\rm gd}^{\omega_{\rm g}}\\ \Delta e_{\rm gq}^{\omega_{\rm g}}\end{bmatrix} + \mathbf{G}'_{\rm ig\omega}\begin{bmatrix}\Delta\omega_{\rm g}\\ 0\end{bmatrix}, \tag{39}$$

where $\mathbf{Y}'_{\rm g}$ and $\mathbf{G}'_{\rm ig\omega}$ are given by

$$\mathbf{Y}'_{\rm g} = [\mathbf{G}'_{e\theta}\mathbf{G}'_{\theta\rm i} + \mathbf{Z}'_{\rm g}]^{-1}[\mathbf{I} - \mathbf{G}'_{e\theta}\mathbf{G}'_{\theta\rm e}], \tag{40}$$

$$\mathbf{G}'_{\rm ig\omega} = -[\mathbf{G}'_{e\theta}\mathbf{G}'_{\theta\rm i} + \mathbf{Z}'_{\rm g}]^{-1}[\mathbf{G}'_{e\omega} + \mathbf{G}'_{e\theta}\mathbf{G}'_{\delta\omega}]. \tag{41}$$

By using a similar approach as the one described for the converter system in the previous sub-section, the small-signal model of the inertial grid based on voltage magnitude and frequency perturbations at the PCC can be obtained in the system *dq*-frame II as

$$\begin{bmatrix}\Delta i_{\rm gd}^{\omega_{\rm g}}\\ \Delta i_{\rm gq}^{\omega_{\rm g}}\end{bmatrix} = \begin{bmatrix}Y'_{\rm g}(1,1) & G'_{\rm ig\omega}(1,1)\\ Y'_{\rm g}(2,1) & G'_{\rm ig\omega}(2,1)\end{bmatrix}\begin{bmatrix}\Delta E_{\rm g}\\ \Delta\omega_{\rm g}\end{bmatrix}. \tag{42}$$

Finally, by utilizing (42) and expressions for active and reactive power injected to the grid, i.e., $P_{\rm g} = e_{\rm gd}^{\omega_{\rm g}} i_{\rm gd}^{\omega_{\rm g}} + e_{\rm gq}^{\omega_{\rm g}} i_{\rm gq}^{\omega_{\rm g}}$, and $Q_{\rm g} = -e_{\rm gd}^{\omega_{\rm g}} i_{\rm gq}^{\omega_{\rm g}} + e_{\rm gq}^{\omega_{\rm g}} i_{\rm gd}^{\omega_{\rm g}}$, the small-signal model of the inertial grid can be expressed in terms of its active and reactive power variations as

$$\begin{bmatrix}\Delta P_{\rm g}\\ \Delta Q_{\rm g}\end{bmatrix} = \overbrace{\begin{bmatrix}E_{\rm g0}Y'_{\rm g}(1,1) + i_{\rm gd0}^{\omega_{\rm g}} & E_{\rm g0}G'_{\rm ig\omega}(1,1)\\ -E_{\rm g0}Y'_{\rm g}(2,1) - i_{\rm gq0}^{\omega_{\rm g}} & -E_{\rm g0}G'_{\rm ig\omega}(2,1)\end{bmatrix}}^{\mathbf{G}'_{\rm tmg}}\begin{bmatrix}\Delta E_{\rm g}\\ \Delta\omega_{\rm g}\end{bmatrix}. \tag{43}$$

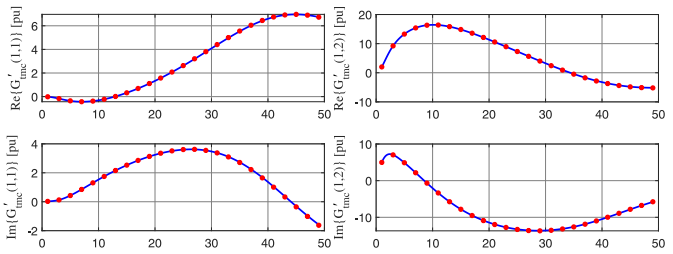

Fig. 6. Frequency response of the first row elements of $\mathbf{G}'_{\text{tmc}}$; analytical model (solid-blue curves) and simulation model (dotted-red curves).

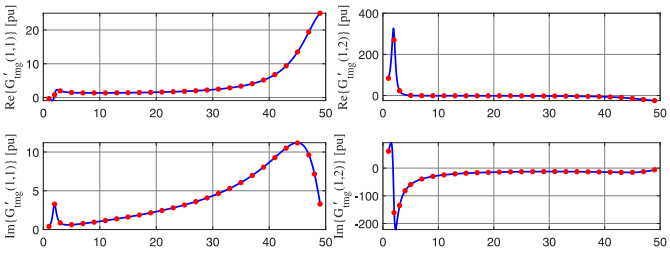

Fig. 7. Frequency response of the first row elements of $\mathbf{G}'_{\text{tmg}}$; analytical model (solid-blue curves) and simulation model (dotted-red curves).

*3) Verification of derived small-signal models:* The analytically derived power-response matrices in the system *dq*-frame II are verified using time-domain simulations. The same methodology as described earlier is used to extract $\mathbf{G}'_{\text{tmc}}$ and $\mathbf{G}'_{\text{tmg}}$ from the simulation tests. The results shown in Fig. 6 and Fig. 7 demonstrate a very good match between the analytical frequency characteristics and those obtained from simulations, verifying the validity of the analytical models.

Furthermore, it can be observed from Fig. 4 - Fig. 7 that frequency characteristics of the respective power-response matrices of the subsystems in the two types of system *dq*-frames are equal, implying that the proposed modeling approach is independent of the reference frame being used for the analysis. This implies that if converter systems are regarded as "black boxes", their aggregation for stability analysis in a multi-converter network can be performed with relative ease using the proposed modeling approach. This is in contrast to the *dq*-impedance-based models, which require complex coordinate transformations for the aggregation of converter systems [12].

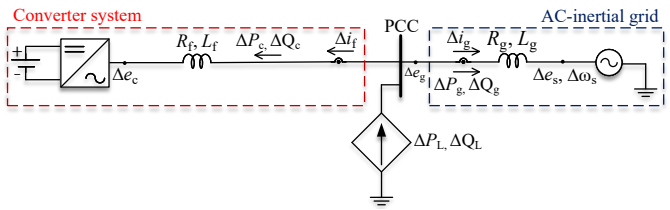


Fig. 8. Applied disturbance to evaluate small-signal stability of grid-connected converter system.

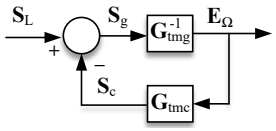


Fig. 9. Equivalent block-scheme describing small-signal characteristics of grid-connected converter system using the proposed modeling approach.

## V. Small-Signal Stability Assessment Criteria

### A. Small-signal stability analysis using the proposed modeling approach

To formulate an assessment criterion for evaluating the small-signal stability of the interconnected system using the proposed modeling approach, a power variation at the PCC, as depicted in Fig. 8, is considered as the source of disturbance. This disturbance results in variations in both the voltage magnitude and fundamental frequency at the PCC, ultimately causing oscillations in the active and reactive powers of the converter system and the inertial grid. By considering the current directions shown in Fig. 8 and using (17) and (25), an equivalent block-scheme (illustrated in Fig. 9) describing the small-signal characteristics of the grid-connected converter system can be obtained. Accordingly, the stability of the system can be assessed by analyzing the poles of the closed-loop transfer matrix, $\mathbf{G}_{\text{cl,prop}}$, which is given by

$$\frac{\mathbf{E}_\Omega}{\mathbf{S}_L} = \mathbf{G}_{\text{cl,prop}} = \left[\mathbf{I} + \mathbf{G}_{\text{tmg}}^{-1}\mathbf{G}_{\text{tmc}}\right]^{-1}\mathbf{G}_{\text{tmg}}^{-1}, \qquad (44)$$

where the matrix, $\mathbf{E}_\Omega$, is as defined in (17) and $\mathbf{S}_L = \mathbf{S}_c + \mathbf{S}_g$.

### B. Small-signal stability analysis using the conventional modeling approach

By using the conventional approach, in which the terminal characteristics of the subsystems are expressed using their corresponding input admittance, the small-signal stability of the interconnected system is assessed by analyzing the poles of the closed-loop transfer matrix, $\mathbf{G}_{\text{cl,conv}}$, which is given by

$$\frac{\mathbf{E}_g}{\mathbf{I}_L} = \mathbf{G}_{\text{cl,conv}} = \left[\mathbf{I} + \mathbf{Y}_g^{-1}\mathbf{Y}_c\right]^{-1}\mathbf{Y}_g^{-1}, \qquad (45)$$

where the matrix, $\mathbf{E}_g$, is as defined in (9) and $\mathbf{I}_L = \mathbf{I}_f + \mathbf{I}_g$.

### C. Comparison of small-signal characteristics

Small-signal characteristics of the grid-connected converter system assessed by two types of modeling approaches are compared in this section. To compare the small-signal characteristics, the poles of the closed-loop transfer matrices $\mathbf{G}_{\text{cl,prop}}$ and $\mathbf{G}_{\text{cl,conv}}$ are obtained and plotted in Fig. 10a) and Fig. 10b), respectively, for two different values of the loop bandwidth of the APC in the converter system.

The figures show that the closed-loop transfer matrices have the same poles, providing the same information about the small-signal stability of the system for the two cases. This is evident from the movement of the poles to the right-hand side of the complex plane in both figures when the loop bandwidth of the APC is increased fourfold, indicating a transition from

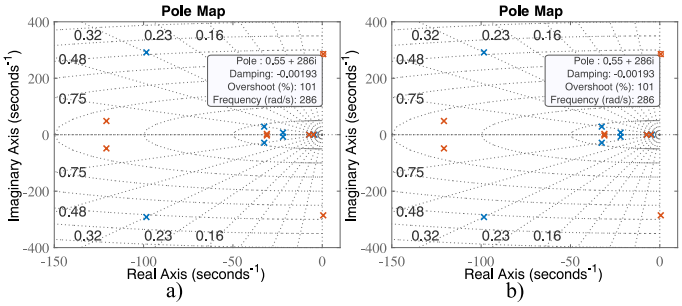


Fig. 10. Poles of closed-loop transfer matrix a) $\mathbf{G}_{\mathrm{cl,prop}}$, b) $\mathbf{G}_{\mathrm{cl,conv}}$ for two different values of loop-bandwidth of APC in converter system. Poles marked by blue color for $\alpha_{\mathrm{pc}} = 2\pi 5$ rad/s, poles marked by red color for $\alpha_{\mathrm{pc}} = 2\pi 20$ rad/s.

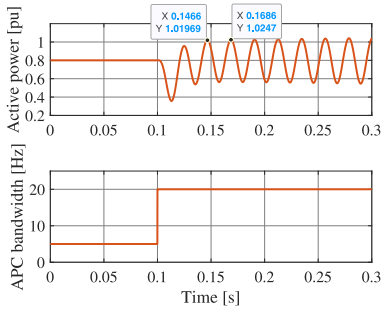


Fig. 11. Impact of the active power controller's loop bandwidth on the active power response of the system.

a stable case (poles in blue) to an unstable case (poles in red). The results of this comparative study imply that the two modeling approaches are equivalent, as they provide the same information regarding the small-signal behavior of the system.

## VI. Simulation Validation of the Stability Assessment

To verify the correctness of the proposed stability assessment criterion, a detailed PSCAD/EMTDC time-domain simulation of the grid-connected converter system shown in Fig. 1 is used. The simulation test is performed using the same operating points mentioned previously and the system and control parameters specified in Table I. Figure 11 shows the time-domain response of the system when the loop bandwidth of the APC in the converter system is varied at $t = 0.1$ s.

It can be observed from the figure that increasing the loop bandwidth of the APC to four times its initial value makes the system unstable, as expected from the theoretical analysis in the previous section. Furthermore, the angular frequency of the growing oscillations matches that of the unstable pole in Fig. 10a) and Fig. 10b). The results obtained from electromagnetic transient simulations thus validate correctness and accuracy of the proposed small-signal models.

## VII. Conclusions

A novel small-signal modeling approach for grid-connected converter systems is presented in this paper. The proposed approach is based on the converter system's power-response matrix, which correlates variations in the active and reactive powers of the converter system with variations in grid voltage magnitude and frequency. This formulation allows a direct assessment of grid services (also referred to as GFM properties) offered by the converter system, such as synthetic inertia, damping provision, and voltage-droop behavior. Moreover, it proves beneficial in analyzing the coupling between active and reactive power responses of the converter system. Furthermore, unlike the conventional impedance-based modeling approach, the proposed approach is independent of the reference frame used for analysis, simplifying aggregation of subsystems regarded as "black boxes" for the small-signal stability assessment of large interconnected systems.

## References


[1] J. Sun, "Small-Signal Methods for AC Distributed Power Systems–A Review," *IEEE Transactions on Power Electronics*, vol. 24, no. 11, Nov. 2009.

[2] L. Harnefors, M. Bongiorno, and S. Lundberg, "Input-Admittance Calculation and Shaping for Controlled Voltage-Source Converters," *IEEE Transactions on Industrial Electronics*, vol. 54, no. 6, Dec. 2007.

[3] B. Wen, D. Boroyevich, R. Burgos, P. Mattavelli, and Z. Shen, "Small-Signal Stability Analysis of Three-Phase AC Systems in the Presence of Constant Power Loads Based on Measured d-q Frame Impedances," *IEEE Transactions on Power Electronics*, vol. 30, no. 10, Oct. 2015.

[4] Z. Liu, J. Liu, D. Boroyevich, R. Burgos, and T. Liu, "Small-signal terminal-characteristics modeling of three-phase droop-controlled inverters," in *2016 IEEE Energy Conversion Congress and Exposition (ECCE)*, Milwaukee, WI, USA: IEEE, Sep. 2016.

[5] Z. Liu, J. Liu, D. Boroyevich, and R. Burgos, "Stability criterion of droop-controlled parallel inverters based on terminal-characteristics of individual inverters," in *2016 IEEE 8th International Power Electronics and Motion Control Conference (IPEMC-ECCE Asia)*, Hefei, China: IEEE, May 2016.

[6] F. Cavazzana, A. Khodamoradi, H. Abedini, and P. Mattavelli, "Analysis of an Impedance Modeling Approach for Droop-Controlled Inverters in System DQ Frame," in *2019 IEEE Energy Conversion Congress and Exposition (ECCE)*, Baltimore, MD, USA: IEEE, Sep. 2019.

[7] S. Wang, Z. Liu, J. Liu, D. Boroyevich, and R. Burgos, "Small-Signal Modeling and Stability Prediction of Parallel Droop-Controlled Inverters Based on Terminal Characteristics of Individual Inverters," *IEEE Transactions on Power Electronics*, vol. 35, no. 1, Jan. 2020.

[8] J. Yu *et al.*, "Accurate Small-Signal Terminal Characteristic Model and SISO Stability Analysis Approach for Parallel Grid-Forming Inverters in Islanded Microgrids," *IEEE Transactions on Power Electronics*, vol. 38, no. 5, May 2023.

[9] M. Yu *et al.*, "Instantaneous penetration level limits of non-synchronous devices in the British power system," *IET Renewable Power Generation*, vol. 11, no. 8, 2017.

[10] National Grid ESO, *Final Modification Report GC0137: Minimum Specification Required for Provision of GB Grid Forming (GBGF) Capability*, Nov. 11, 2021.

[11] A. Narula, "Grid-forming wind power plants," Ph.D. dissertation, Mar. 2023.

[12] Q. Xiao, P. Mattavelli, A. Khodamoradi, and F. Tang, "Analysis of transforming dq impedances of different converters to a common reference frame in complex converter networks," *CES Transactions on Electrical Machines and Systems*, vol. 3, no. 4, 2019.